Supporting Information for Isostructurality of Quinoxaline Crystal Phases: The Interplay of Weak Hydrogen Bonds and Halogen Bonding

1. Conformation of Molecular Structures

Table S1. Crystallographic Data for Samples.

Identification code	**Q3,3'F_2**	**Q,3,3'Cl_2**	**Q3,3'I_2**	**Q3,3'Me_2**
Empirical formula	$C_{20}H_{12}F_2N_2$	$C_{20}H_{12}Cl_2N_2$	$C_{20}H_{12}I_2N_2$	$C_{22}H_{18}N_2$
Formula weight	318.32	351.22	534.12	310.38
Temperature/K	99.82	296.15	99.87	99.78
Crystal system	monoclinic	monoclinic	monoclinic	monoclinic
Space group	$P2_1/n$	$P2_1/n$	$P2_1/n$	$P2_1/n$
a/Å	12.7621(18)	13.368(3)	8.6398(5)	12.313(4)
b/Å	7.6916(9)	7.5374(12)	19.4072(10)	7.563(2)
c/Å	15.439(2)	16.175(4)	10.7039(6)	17.916(5)
α/°	90	90	90	90
β/°	101.230(7)	104.640(9)	101.237(3)	102.333(11)
γ/°	90	90	90	90
Volume/$Å^3$	1486.5(3)	1576.9(5)	1760.36(17)	1630.0(8)
Z	4	4	4	4
$\rho_{calc}g/cm^3$	1.422	1.479	2.015	1.265
μ/mm^{-1}	0.102	0.414	3.576	0.074
F(000)	656.0	720.0	1008.0	656.0
Crystal size/mm^3	0.38 × 0.21 × 0.13	0.75 × 0.54 × 0.10	0.47 × 0.1 × 0.1	0.53 × 0.12 × 0.1
Radiation	MoKα (λ = 0.71073)	MoKα (λ = 0.71073)	MoKα (λ = 0.71073)	MoKα (λ = 0.71073)
2Θ range for data collection/°	5.38 to 61.156	5.206 to 60.94	5.246 to 70.882	5.868 to 61.1
Index ranges	-18 ≤ h ≤ 18 -8 ≤ k ≤ 10 -22 ≤ l ≤ 22	-17 ≤ h ≤ 14 -8 ≤ k ≤ 10 -11 ≤ l ≤ 20	-13 ≤ h ≤ 13 -28 ≤ k ≤ 31 -17 ≤ l ≤ 17	-17 ≤ h ≤ 17 -10 ≤ k ≤ 10 -24 ≤ l ≤ 25
Reflections collected	22288	8785	39187	22160
Independent reflections	4452 [R_{int} = 0.1004, R_{sigma} = 0.1129]	3565 [R_{int} = 0.0402, R_{sigma} = 0.0774]	7651 [R_{int} = 0.0564, R_{sigma} = 0.0600]	4920 [R_{int} = 0.0977, R_{sigma} = 0.0973]
Data/restraints/parameters	4452/0/265	3565/0/265	7651/0/217	4920/0/289
Goodness-of-fit on F^2	1.018	1.012	1.022	1.036
Final R indexes [I>=2σ (I)]	R_1 = 0.0592, wR_2 = 0.1002	R_1 = 0.0450, wR_2 = 0.0847	R_1 = 0.0461, wR_2 = 0.0947	R_1 = 0.0850 wR_2 = 0.2017
Final R indexes [all data]	R_1 = 0.1424, wR_2 = 0.1237	R_1 = 0.0917, wR_2 = 0.1008	R_1 = 0.0854, wR_2 = 0.1067	R_1 = 0.1509 wR_2 = 0.2449
Largest diff. peak/hole / e $Å^{-3}$	0.33/-0.33	0.34/-0.35	2.95/-1.61	0.75/-0.42

2D-NOESY NMR Spectra

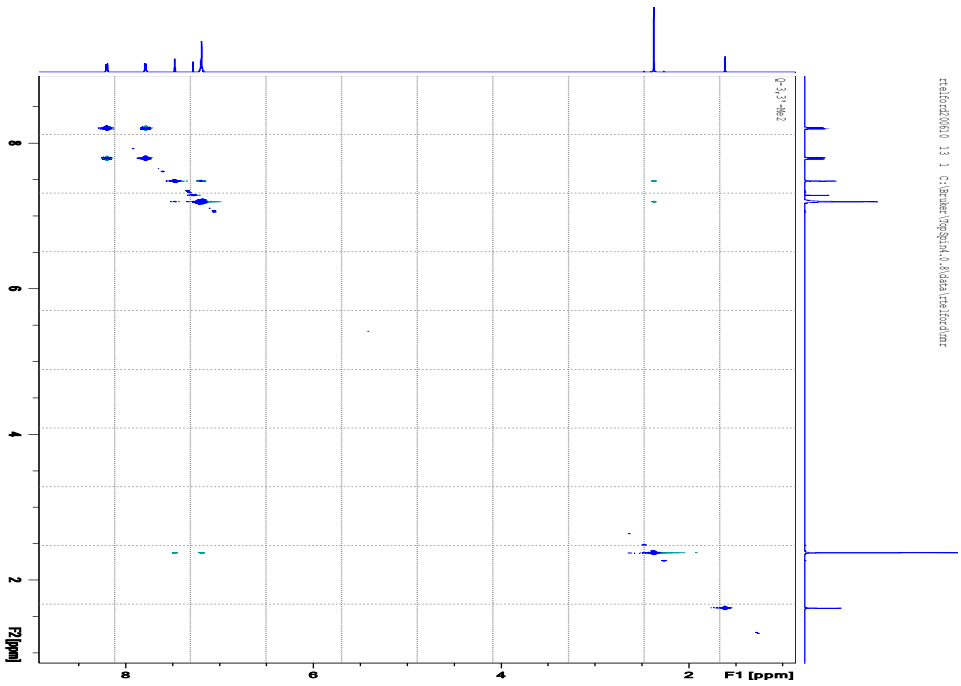

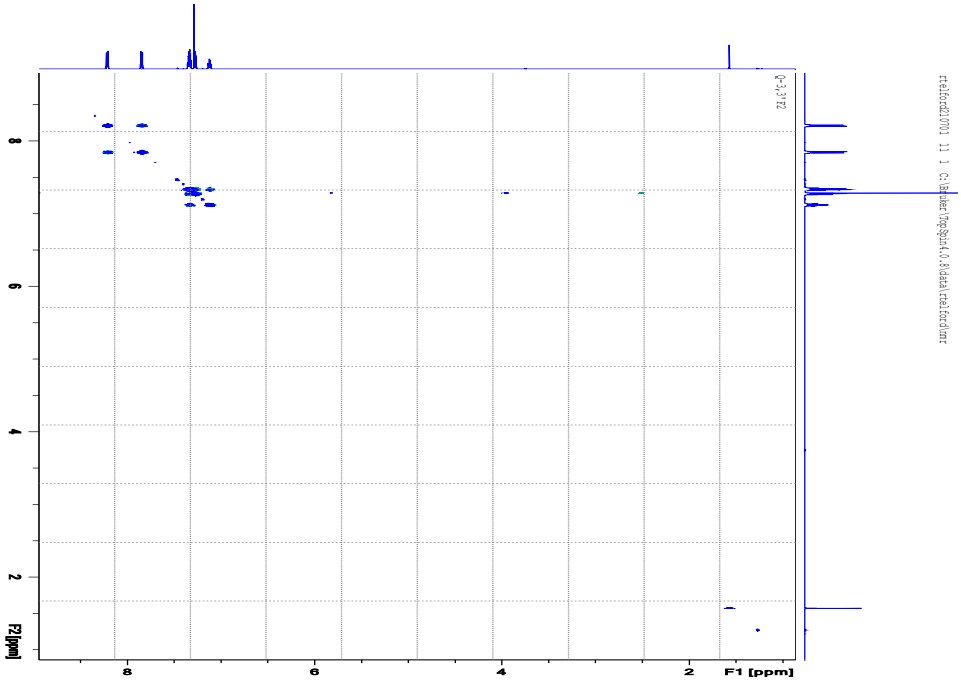
F2 [ppm]
8
6
4
2
F1 [ppm]

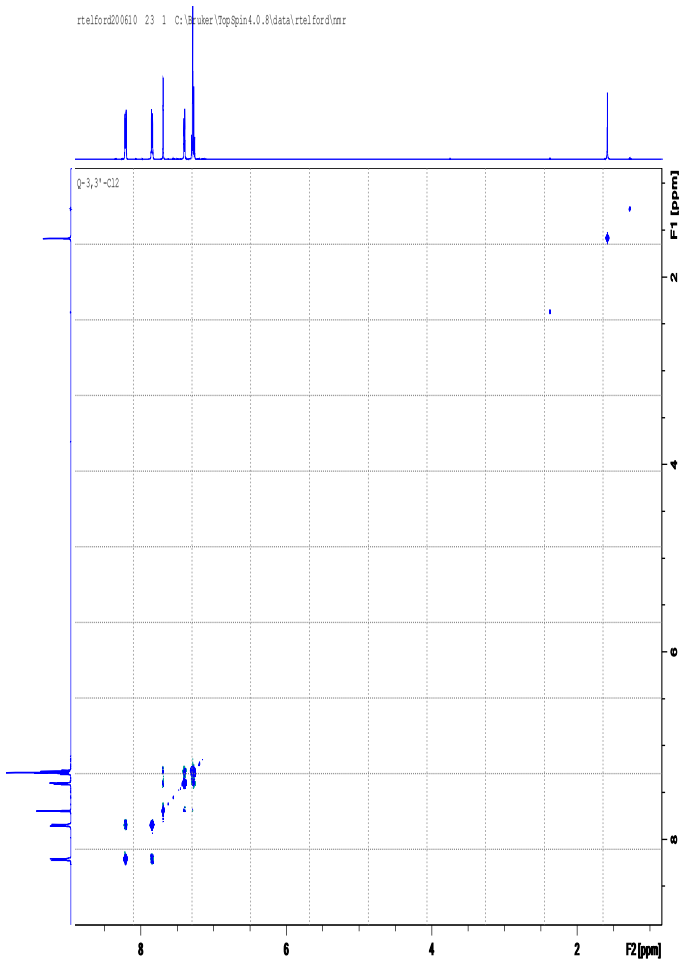
rtelford200610 23 1 C:\Bruker\TopSpin4.0.8\data\rtelford\nmr
Q-3,3*-C12
F1 [ppm]
2
4
6
8
8
6
4
2
F2 [ppm]

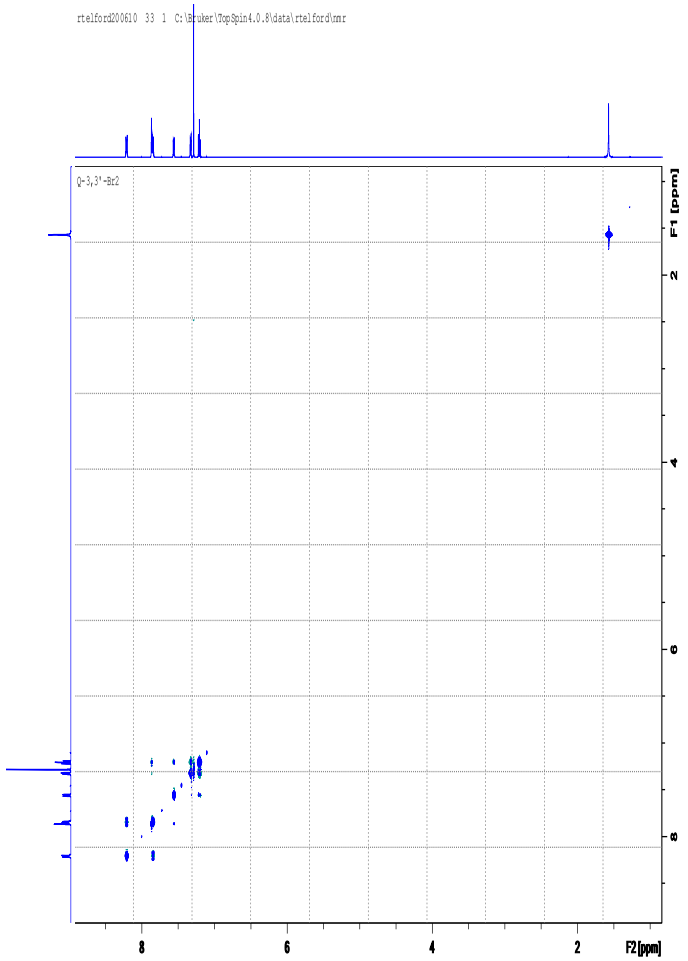
rtelford200610 33 1 C:\Bruker\TopSpin4.0.8\data\rtelford\nmr
Q-3,3'-Br2
F1 [ppm]
2
4
6
8
8
6
4
2
F2 [ppm]

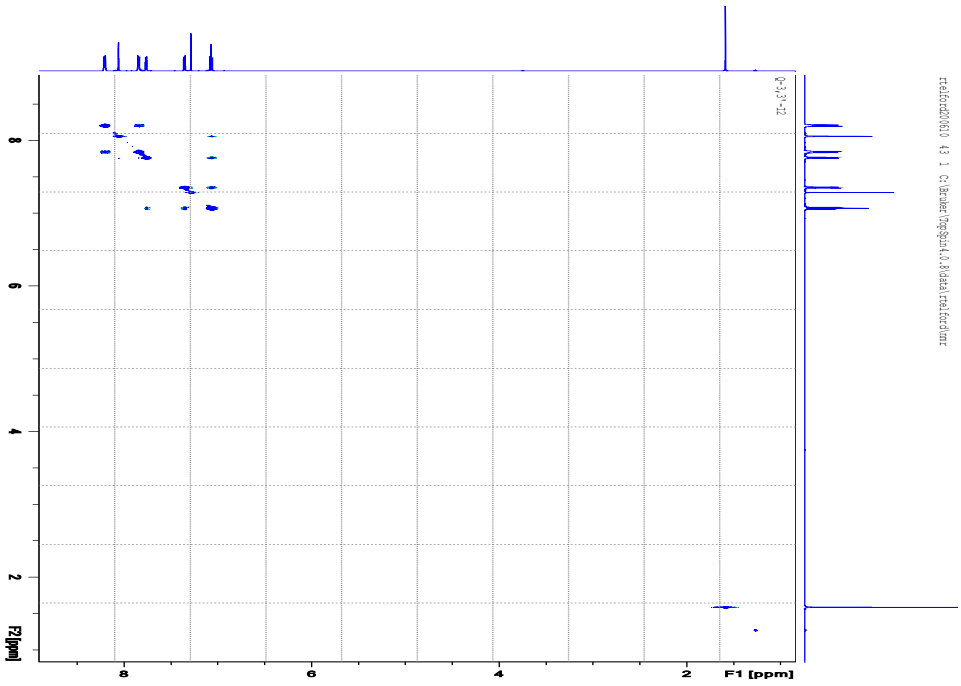

Figure S1. NOESY NMR data obtained from **Q3,3'Me$_2$, Q3,3'F$_2$, Q3,3'Cl$_2$, Q3,3'Br$_2$ and Q3,3'I$_2$**

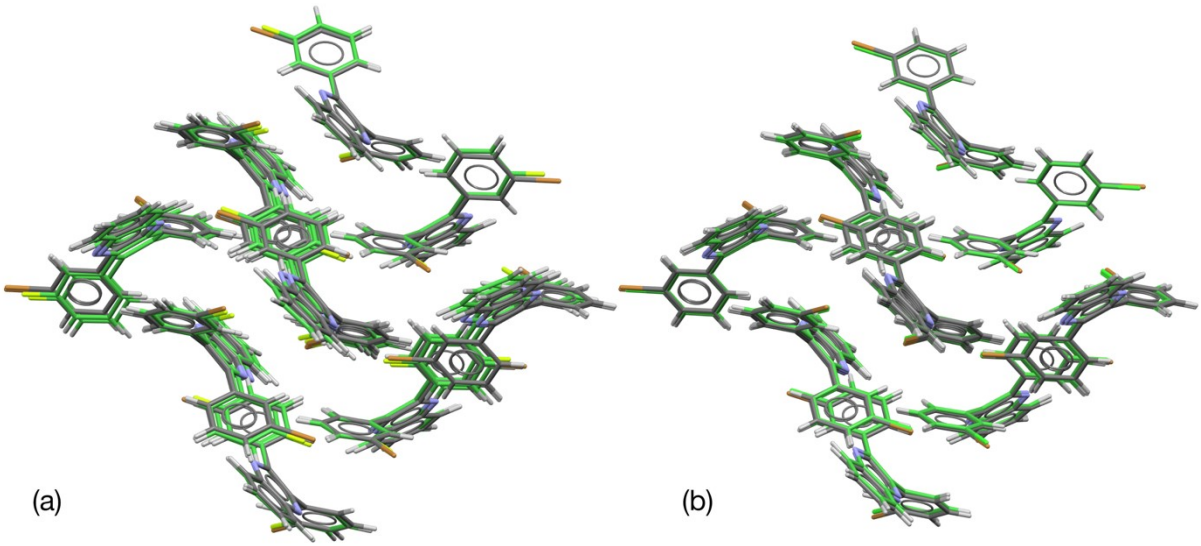

Figure S2. Overlay of the crystal structure of **Q3,3'Br$_2$** with those of (a) **Q3,3'F$_2$** and (b) **Q3,3'Cl$_2$** showing the isostructurality of the three structures. The **Q3,3Br$_2$** structure has grey

carbon atoms while the other structures shown with green carbon atoms. Both images are viewed along the a-axis of the crystals.

2. Conformation of Polymorphism

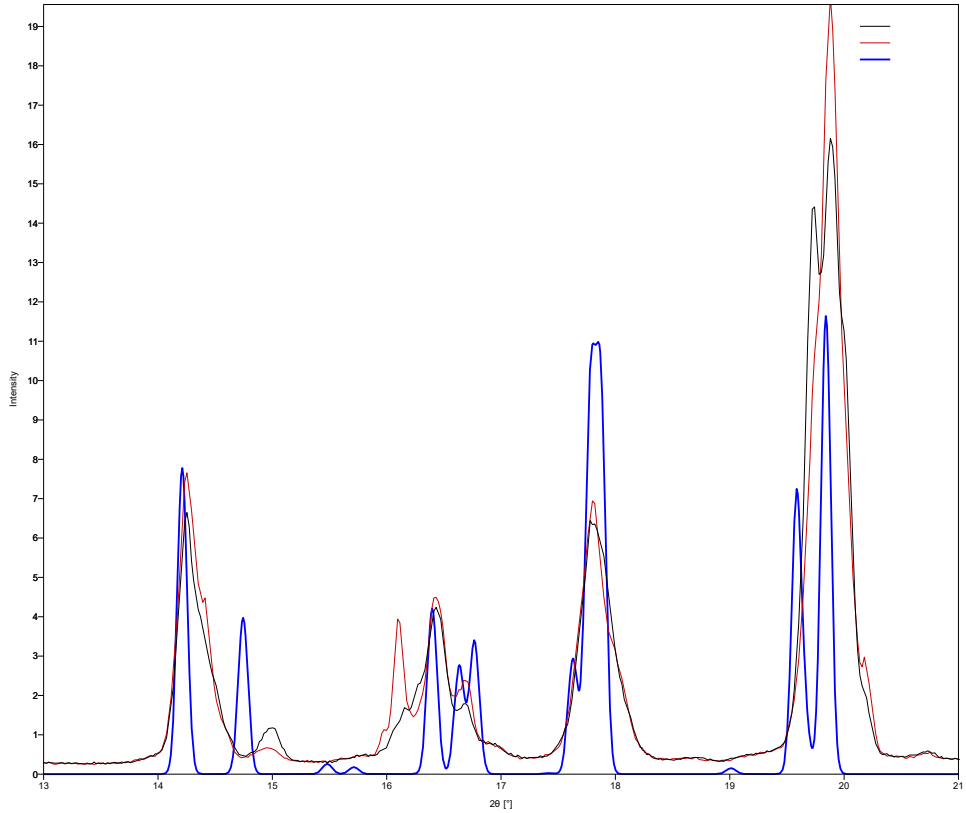

Figure S3. Comparison of **Q3,3'H_2** PXRD data. Simulated data from single crystal structure (ODEJAJ, blue line), experimental data of two samples (black and red lines).

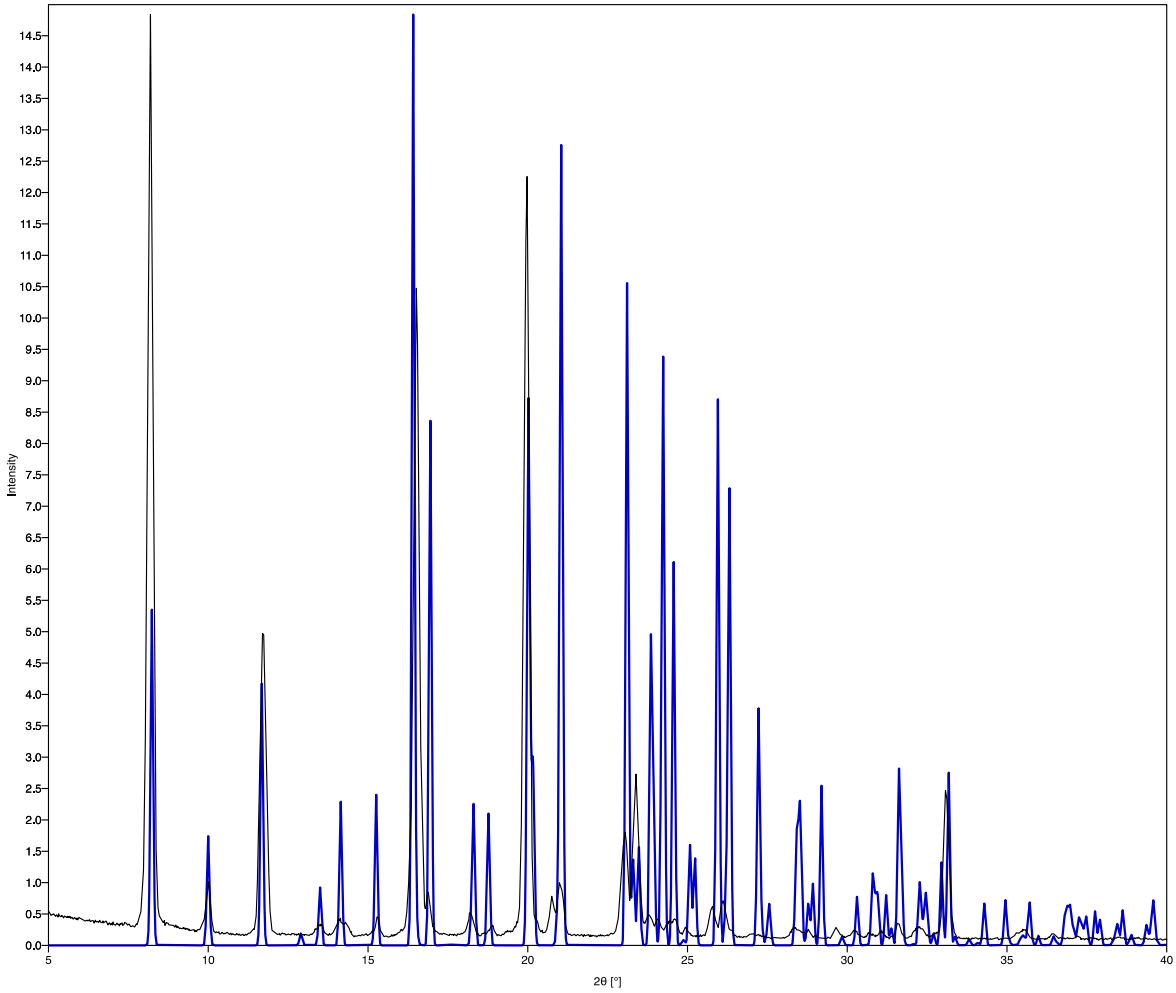

Figure S4. Comparison of PXRD patterns for **Q3,3'F_2** recrystallised from pet. ether and simulated from single crystal structure.

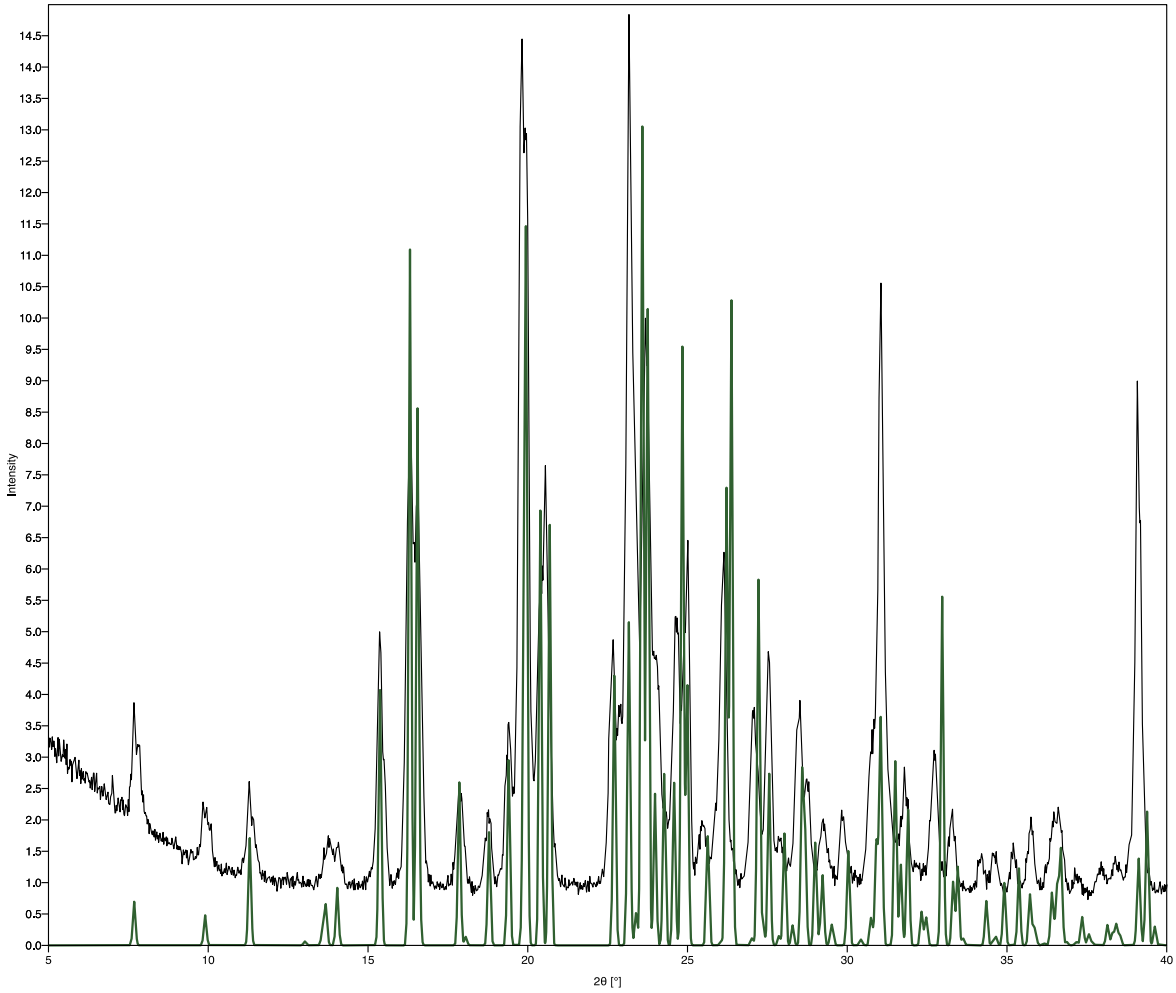

Figure S5. Comparison of PXRD patterns for **Q3,3'Cl$_2$** recrystallised from pet. ether and simulated from single crystal structure.

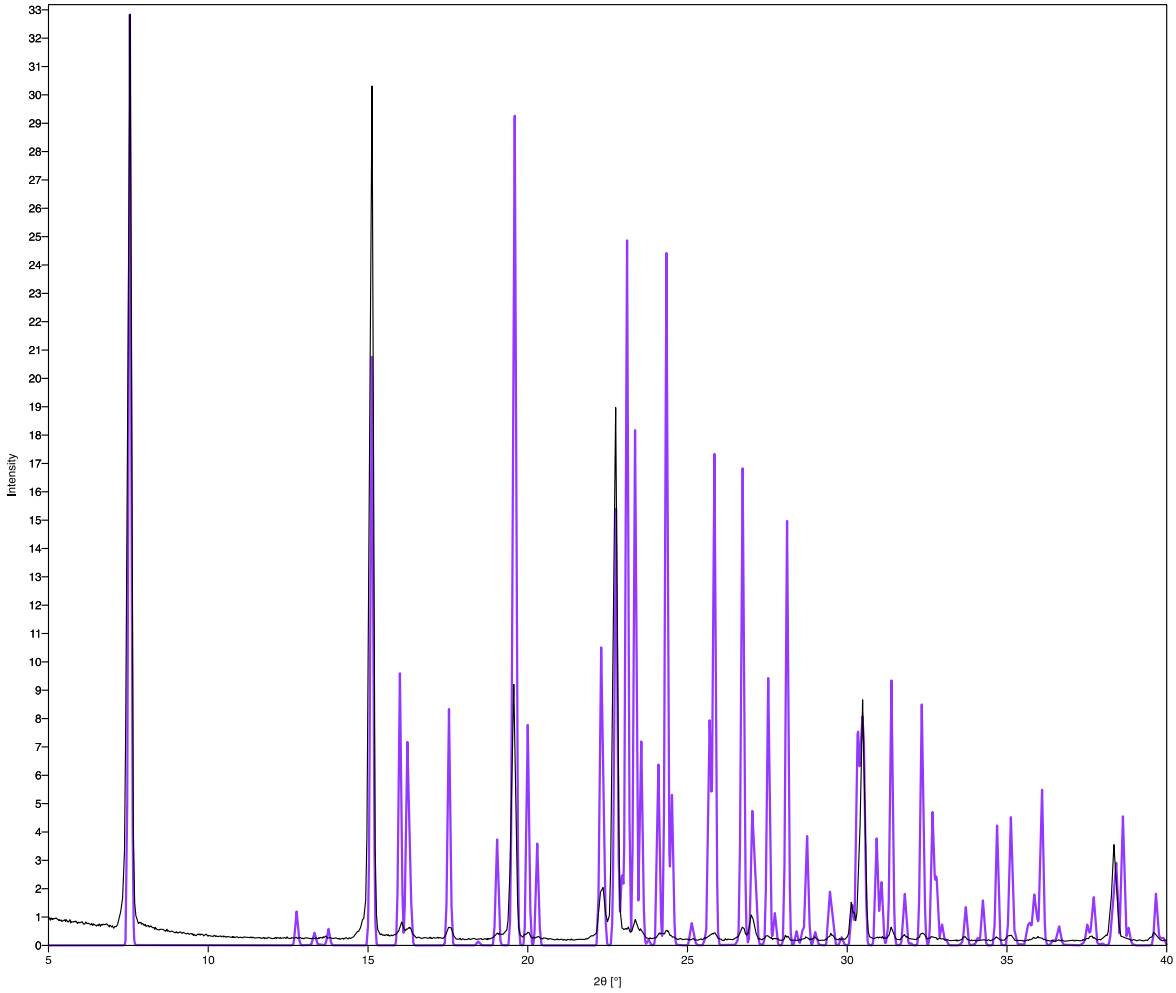

Figure S6. Comparison of PXRD patterns for **Q3,3'Br$_2$** recrystallised from pet. ether and simulated from single crystal structure.

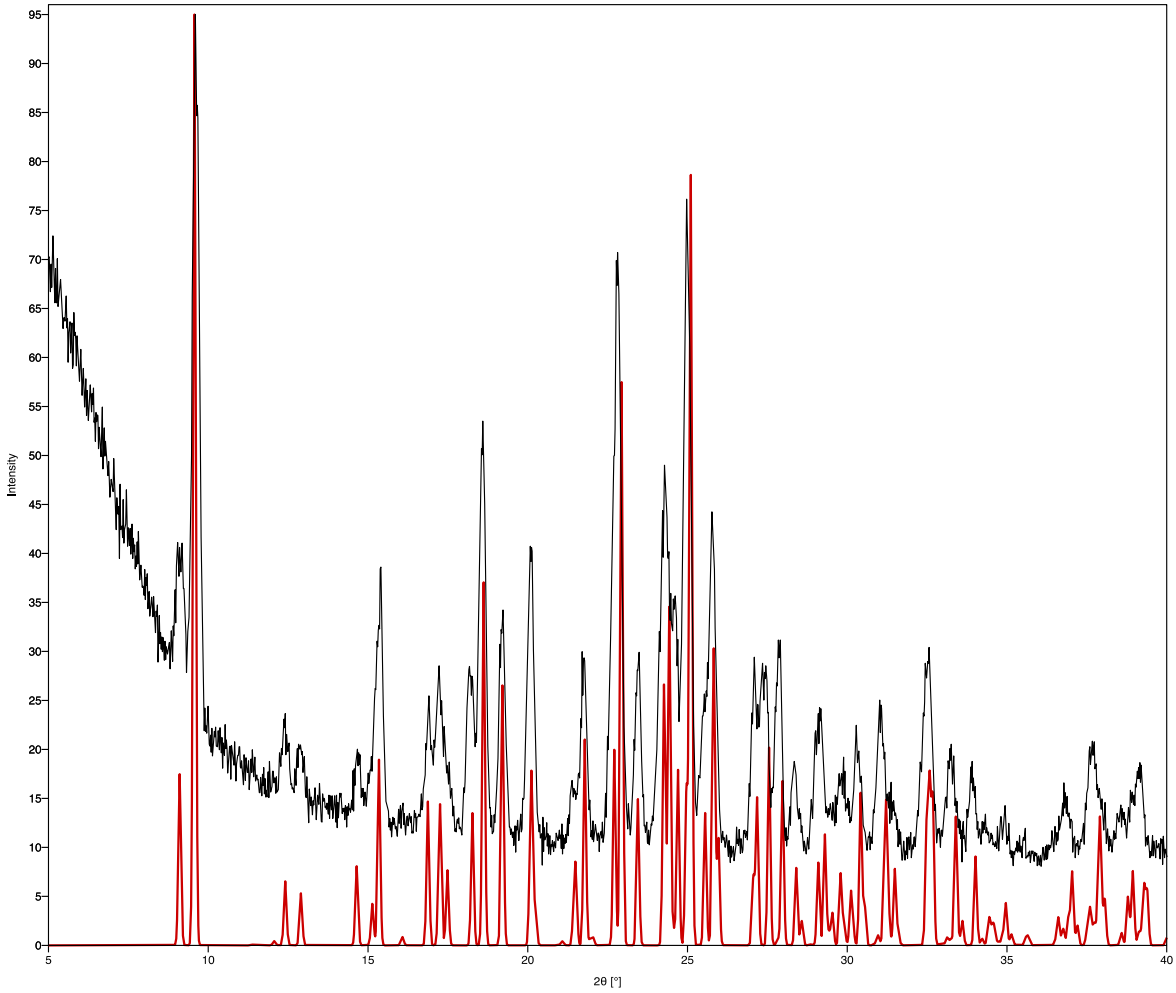

Figure S7. Comparison of PXRD patterns for **Q3,3'Br$_2$** recrystallised from Pet. Ether and simulated from single crystal structure.

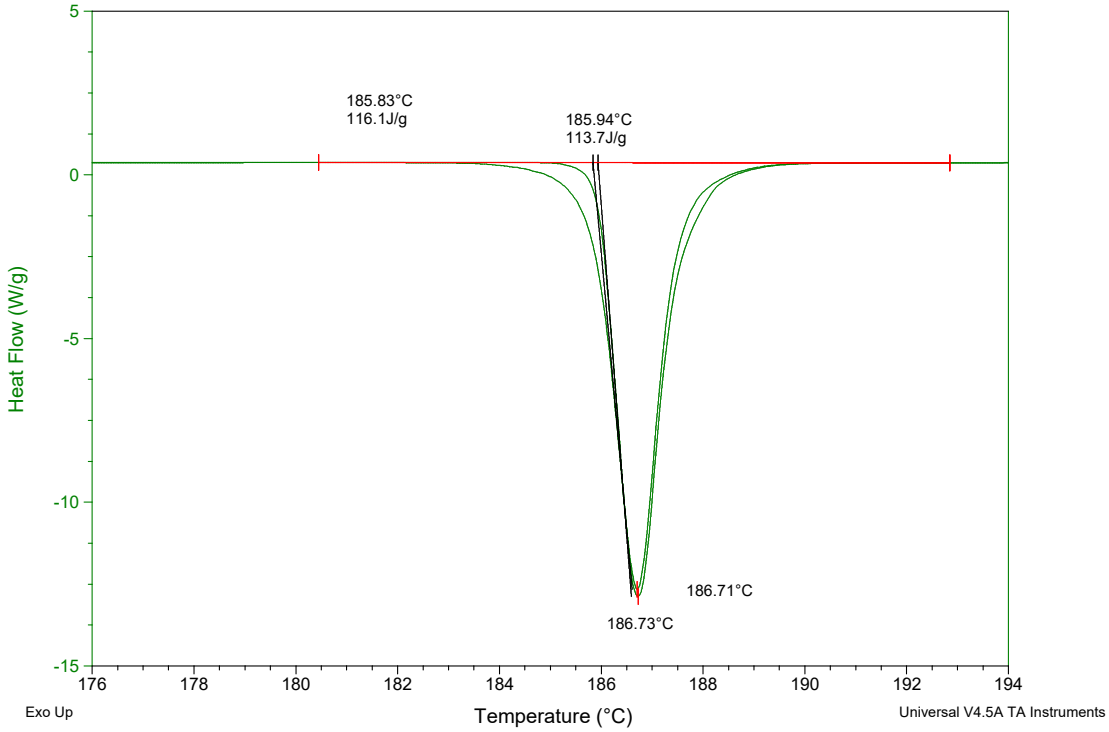

Figure S8. DSC trace for the first and second heating cycles of **Q3,3'Cl$_2$**.

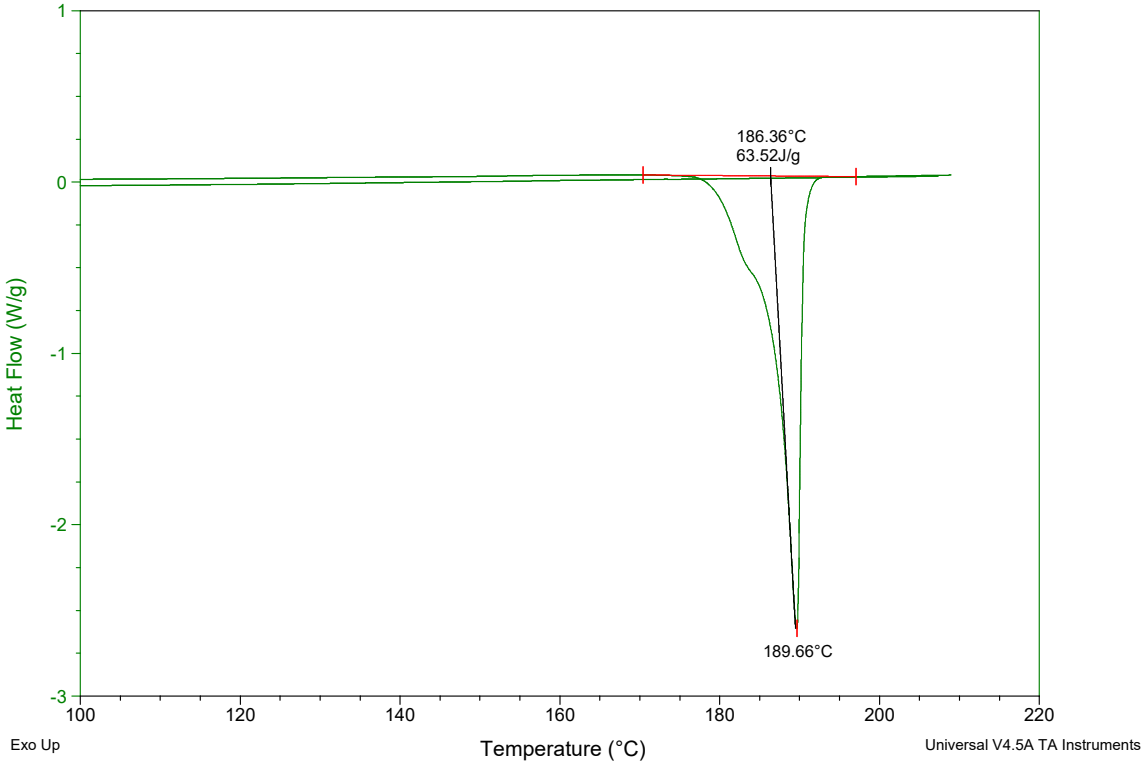

Figure S9. DSC trace for the first and second heating cycles of **Q3,3'I$_2$**.